Mechanics Research Communications 105 (2020) 103515

Contents lists available at ScienceDirect

Mechanics Research Communications

journal homepage: www.elsevier.com/locate/mechrescom

Coarse–grained model based on rigid grains interaction for single layer molybdenum disulfide

A.Yu. Panchenko[a], E.A. Podolskaya[b,c], I.E. Berinskii[a,*]

[a] School of Mechanical Engineering, Tel Aviv Univeristy, Ramat Aviv, Tel Aviv 69978, Israel
[b] Peter the Great St. Petersburg Polytechnic University, 29, Politechnicheskaya str., St. Petersburg 195251, Russia
[c] Institute for Problems in Mechanical Engineering RAS, 61, Bolshoy pr. V. O., St. Petersburg 199178, Russia

ARTICLE INFO

Article history:
Received 16 December 2019
Revised 16 March 2020
Accepted 16 March 2020
Available online 21 March 2020

Keywords:
Molybdenum disulfide
Coarse–grained simulations
Particle dynamics method
Phonon spectrum
Nanoindentation

ABSTRACT

Single–layer molybdenum disulfide ($SLMoS_2$) is a promising two–dimensional material with a wide range of possible applications in NEMS. Traditional molecular dynamics (MD) simulations of $SLMoS_2$ are very time–consuming and cannot be applied to the real microscopic–level systems. We develop a coarse–grained model combining the atoms of crystal lattice into rigid 'grains'. The interaction between the grains is based on Stillinger–Weber potential with parameters recalculated to fulfill the elastic properties of the original lattice. The model is applied to calculate the phonon spectrum and for the nanoindentation problem. It is shown that in the case of small strains the model is as accurate as regular MD simulations, but uses much less interatomic interactions; hence, it is much more time–efficient.

1. Introduction

Single–layer molybdenum disulfide ($SLMoS_2$) has recently emerged as a promising 2D material due to its exceptional mechanical and piezoelectric properties. Unlike graphene, the most famous 2D material consisting of carbon atoms combined in one planar layer, $SLMoS_2$ is a part of hexagonal close-packed (HCP) structure, having three layers in the orthogonal direction. The structure leads to the difference of properties of this two materials, as it is discussed in the review paper of Jiang [8]; for example, the Young modulus of $SLMoS_2$ reported to be equal Y = 180 N/m which is smaller than that of graphene (Y = 335.0 N/m). However, the bending rigidity of $SLMoS_2$ is much higher as well as its Q-factor (ability to preserve the oscillations). Also, whereas graphene has an outstanding electrical conductivity, $SLMoS_2$ is a semiconductor with a direct band gap which makes it applicable for single–layered nanoelectronic devices such as transistors [14] and memory cells [4]. The combination of these properties gives opportunities for using the single-layer molybdenum disulfide in nanoelectromechanical systems (NEMS).

NEMS developing is not possible without the accurate computational simulations. Usually, molecular dynamics simulations are used to describe large displacements and strains of $SLMoS_2$ during the stretching [11] or mechanical indentation [15,20]. Often, the Stillinger-Webber (SW) potential is applied for such kind of simulations. This potential allows to describe the non–linear mechanical effects, but keeps the numerical simulations at a relatively fast level. Unfortunately, such kind of simulations are still very time-consuming, so many phenomena of large-sized $SLMoS_2$ usually observed in nanomechanical experiments cannot be theoretically investigated using standard MD methods. To overcome these issues, the coarse–grained approach was proposed in [18] to simulate folding of single-layer MoS_2 modeled as a chain of grains. The interactions between the grains were described using various simplified potentials with the parameters derived from the SW potential for the original MoS_2 structure. The advanced 2D model was proposed in [19]. In this work, the original atomic structure is substituted by the structure of the bounded grains, such that every grain corresponds to the specific number of the *Mo* or *S* atoms and the hexagonal structure is maintained. The grains are interacting with the SW potential as well as in original atomic structure, but new parameters are determined basing on valence force field (VFF) model.

We propose another way to simulate the atomistic structure using the coarse-grained (CG) modeling: we do not substitute one lattice by another one, instead, we combine atoms of the lattice into 'grains'. The grain combines three unit cells of the $SLMoS_2$ hexagonal close-packed (HCP) structure, which is infinite in the plane of transverse isotropy and has only three layers in the orthogonal direction. The top and bottom layers are occupied by sulfur (*S*) and the medium layer consists of molybdenum (*Mo*). As a

* Corresponding author.
E-mail address: igorbr@tauex.tau.ac.il (I.E. Berinskii).

https://doi.org/10.1016/j.mechrescom.2020.103515
0093-6413/

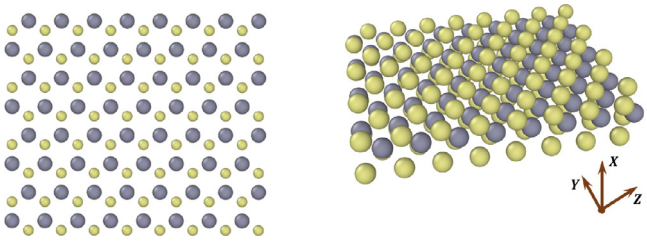

Fig. 1. Crystal lattice of MoS_2, visualized using OVITO software [16].

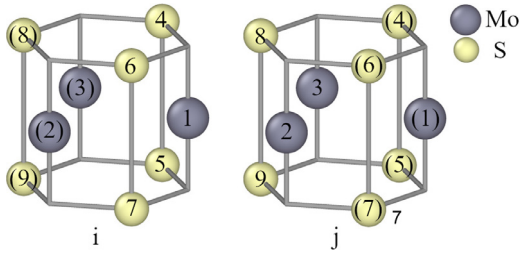

Fig. 2. Pair of interacting grains of MoS_2.

result, the grains form a two-dimensional triangular lattice. Unlike previous approaches, we consider the grains not as material points, but as the rigid bodies, taking their rotational degrees of freedom into account. In this case, a specific potential has to be developed to add torques arising between the grains to the forces of interaction. Such type of potential was used before for the original $SLMoS_2$ crystal lattice [3], but not for the CG structure.

The paper is organized as follows. First, the grains in lattice are introduced and the forces and torques between the grains are calculated using the potentials of interaction between the atoms. Then, the parameters of SW potential are re-calibrated so that new material fulfills the elastic moduli of the original lattice. Then, the test problems are considered: phonon dispersion and nanoindentation.

2. Grains in MoS_2 and their interaction

The structure of $SLMoS_2$ is geometrically imperfect, as the distance between *Mo* and *S* is smaller than distances $Mo-Mo$ and $S-S$. Each *Mo* has twelve neighboring atoms, i.e. six *Mo* in the plane of isotropy and six *S* above and beneath (Fig. 1). We choose grains in the lattice in such a manner, so that any of them contain 3 atoms of *Mo* and 6 atoms of *S* (Fig. 2). The grains are considered as the rigid bodies, so atoms are 'freezed' inside the grain. As a result, the center of mass of the grain is located in the center of the hexagonal prism and the inertia tensor $\mathbf{\Theta_i}$ has a diagonal form (1):

$$m = 480.248\text{u}$$
$$\Theta_\text{i} = \begin{pmatrix} 1257.96 & 0 & 0 \\ 0 & 1257.96 & 0 \\ 0 & 0 & 1525.39 \end{pmatrix} \text{uÅ}^2 \tag{1}$$

Even such small grains approach leads to the reduction of the number of calculated interactions: the number of interactions per grain decreases from 9 to 6 for $Mo-Mo$, from 18 to 12 for $S-S$, from 18 to 6 for $Mo-S$, from 27 to 15 for $Mo-S-S$, from 18 to 12 for $S-Mo-Mo$. It should be noted that for 12 three-atom interactions $Mo-S-S$ and 12 $S-Mo-Mo$ a pair of atoms belong to the same grain, and the distance between them remains constant, which also further reduces the number of calculated values. Thus, on average, the number of calculated interactions decreases by the factor of 1.76. When atoms are combined into a grain, the number of degrees of freedom decreases from 27 to 6 per grain. However, 70% of the calculation time is consumed by the calculation of interactions, thus, the calculation acceleration upon transition to grains is approximately 1.7 times. It should also be noted that the size of the grain can be scaled so that the shape of the grain will be preserved. For example, seven grains shown in Fig. 3 can be combined into the one, which will significantly decrease the interactions number.

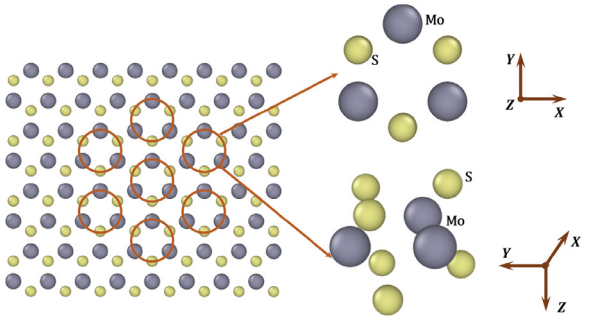

Fig. 3. Grains in MoS_2 lattice.

We are going to determine the potential of interaction between the grains. First, we will obtain the forces and torques acting on the grain relative to its center of mass. To do it, let us consider the interactions between the specific atoms. First, consider the pair bonding. The potential of interaction can be represented as a function of the position vector $\Pi_{\alpha\beta}(\mathbf{r}_{\alpha\beta})$ between two atoms (see (36) in Appendix for the details). The parameters of the potential B, σ, a, and ε are different for three types of interaction: $Mo-Mo$, $S-S$, and $Mo-S$. The distance between two particles α and β is given by

$$r_{\alpha\beta} = |\mathbf{r}_{\alpha\beta}|, \qquad \mathbf{r}_{\alpha\beta} = \mathbf{r}_\beta - \mathbf{r}_\alpha \tag{2}$$

Here and after, vectors and tensors are denoted by the bold symbols. The force of pair interaction $\mathbf{F}^2_{ij}$ acting to the grain i from the grain j can be found as a sum of forces $\mathbf{F}^2_\alpha$ acting to the atoms α from the atoms β, where $\alpha = 1, 4, 5, 6, 7$ and $\beta = 2, 3, 8, 9$. Consider $\mathbf{F}^2_\alpha$:

$$\mathbf{F}^2_\alpha = -\sum_\beta \frac{\partial \Pi_{\alpha\beta}}{\partial \mathbf{r}_\alpha} = \sum_\beta \frac{\partial \Pi_{\alpha\beta}}{\partial \mathbf{r}_{\alpha\beta}} = \sum_\beta \mathbf{F}^2_{\alpha\beta}, \tag{3}$$

where it is denoted that $\mathbf{F}^2_{\alpha\beta} = \frac{\partial \Pi_{\alpha\beta}}{\partial \mathbf{r}_{\alpha\beta}}$. Hence, the total force

$$\mathbf{F}^2_{ij} = -\mathbf{F}^2_{ji} = \mathbf{F}^2_{Mo-S} + \mathbf{F}^2_{Mo-Mo} + \mathbf{F}^2_{S-S}, \tag{4}$$

where

$$\mathbf{F}^2_{Mo-S} = \mathbf{F}^2_{18} + \mathbf{F}^2_{19}, \qquad \mathbf{F}^2_{Mo-Mo} = \mathbf{F}^2_{12} + \mathbf{F}^2_{13}$$
$$\mathbf{F}^2_{S-S} = \mathbf{F}^2_{48} + \mathbf{F}^2_{68} + \mathbf{F}^2_{59} + \mathbf{F}^2_{79} \tag{5}$$

Now let us determine the torques between the grains. Let us define $\mathbf{r}_i$ as a vector directed to the center of mass of the grain i. The torque acting to the grain i from the grain j and calculated relative to the center of mass of i is

$$\mathbf{M}^2_{ij} = \sum_{\alpha,\beta} \mathbf{r}_{i\alpha} \times \mathbf{F}^2_{\alpha\beta} = \sum_{\alpha,\beta} \mathbf{r}_{i\beta} \times \mathbf{F}^2_{\alpha\beta} \tag{6}$$

For our specific α and β

$$\mathbf{M}^2_{ij} = \mathbf{r}_{i1} \times (\mathbf{F}^2_{18} + \mathbf{F}^2_{19} + \mathbf{F}^2_{12} + \mathbf{F}^2_{13}) + \mathbf{r}_{i8} \times (\mathbf{F}^2_{48} + \mathbf{F}^2_{68}) + \mathbf{r}_{i9} \times (\mathbf{F}^2_{59} + \mathbf{F}^2_{79}) \tag{7}$$

Considering a torque acting to the second grain one can obtain

$$\mathbf{M}^2_{ji} = -\mathbf{r}_{j1} \times (\mathbf{F}^2_{18} + \mathbf{F}^2_{19} + \mathbf{F}^2_{12} + \mathbf{F}^2_{13})$$

$$-\mathbf{r}_{j8}\times(\mathbf{F}^2_{48}+\mathbf{F}^2_{68})-\mathbf{r}_{j9}\times(\mathbf{F}^2_{59}+\mathbf{F}^2_{79}) \tag{8}$$

One can notice that the distance between the centers of masses of grains can be represented as

$$\mathbf{r}_{ij}=\mathbf{r}_{i1}-\mathbf{r}_{j1}=\mathbf{r}_{i8}-\mathbf{r}_{j8}=\mathbf{r}_{i9}-\mathbf{r}_{j9}. \tag{9}$$

Using this one can check that (7) and (8) satisfy to the 3rd Newton's law for torques:

$$\mathbf{M}^2_{ij}+\mathbf{M}^2_{ji}=\mathbf{r}_{ij}\times\mathbf{F}^2_{ij} \tag{10}$$

As a second step the three–body (angle bending) interaction $\Pi^3_{\alpha\beta\gamma}(\mathbf{r}_{\alpha\beta},\mathbf{r}_{\alpha\gamma})$ was taken into account (see (37) in Appendix for the details). The interaction energy between two grains is found as

$$\begin{aligned}\Pi^3 &= \Pi^3_{Mo-S-S}+\Pi^3_{S-Mo-Mo},\\ \Pi^3_{Mo-S-S} &= \Pi^3_{189}+\Pi^3_{179}+\Pi^3_{159}+\Pi^3_{168}+\Pi^3_{148},\\ \Pi^3_{S-Mo-Mo} &= \Pi^3_{812}+\Pi^3_{813}+\Pi^3_{912}+\Pi^3_{913}\end{aligned} \tag{11}$$

The three–body potentials of interaction $\Pi^3_{\alpha\beta\gamma}(\mathbf{r}_\alpha,\mathbf{r}_\beta,\mathbf{r}_\gamma)$ have the form (37), where

$$\begin{aligned}\mathbf{r}_{\alpha\beta} &= \mathbf{r}_\beta-\mathbf{r}_\alpha,\quad \mathbf{r}_{\alpha\gamma}=\mathbf{r}_\gamma-\mathbf{r}_\alpha,\\ \cos\Theta_{\alpha\beta\gamma} &= \frac{\mathbf{r}_{\alpha\beta}\cdot\mathbf{r}_{\alpha\gamma}}{r_{\alpha\beta}r_{\alpha\gamma}},\quad r=|\mathbf{r}|.\end{aligned} \tag{12}$$

Next, we calculate the forces acting to the grains i and j caused by these interactions. Consider the force acting to the central particle α due to a single interaction $\Pi_{\alpha\beta\gamma}$:

$$\mathbf{F}^3_\alpha=\mathbf{F}^3_\beta+\mathbf{F}^3_\gamma,\quad \mathbf{F}^3_\beta=\frac{\partial\Pi^3_{\alpha\beta\gamma}}{\partial\mathbf{r}_{\alpha\beta}},\quad \mathbf{F}^3_\gamma=\frac{\partial\Pi^3_{\alpha\beta\gamma}}{\partial\mathbf{r}_{\alpha\gamma}}. \tag{13}$$

Using this, it is possible to calculate the sum of the forces acting to the grain i:

$$\mathbf{F}^3_{ij}=\mathbf{F}^3_1+\mathbf{F}^3_4+\mathbf{F}^3_5+\mathbf{F}^3_6+\mathbf{F}^3_7. \tag{14}$$

From (13) follows that the contribution from the 3–body interaction to the atoms 4–7 is zero because of the fixed distances between the respective atoms and atom 1. Consequently

$$\mathbf{F}^3_{ij}=\mathbf{F}^3_1=\mathbf{F}^3_{Mo-S-S}+\mathbf{F}^3_{S-Mo-Mo}, \tag{15}$$

where

$$\begin{aligned}\mathbf{F}^3_{Mo-S-S} &= \frac{\partial(\Pi^3_{148}+\Pi^3_{168}+\Pi^3_{189})}{\partial\mathbf{r}_{18}}+\frac{\partial(\Pi^3_{159}+\Pi^3_{179}+\Pi^3_{189})}{\partial\mathbf{r}_{19}}\\ \mathbf{F}^3_{S-Mo-Mo} &= \frac{\partial(\Pi^3_{812}+\Pi^3_{813})}{\partial\mathbf{r}_{18}}+\frac{\partial(\Pi^3_{912}+\Pi^3_{913})}{\partial\mathbf{r}_{19}}\end{aligned} \tag{16}$$

Consideration of the force acting to the second grain gives

$$\mathbf{F}^3_{ji}=\mathbf{F}^3_2+\mathbf{F}^3_3+\mathbf{F}^3_8+\mathbf{F}^3_9. \tag{17}$$

It may be noted, that the contribution from the 3–body interaction to the atoms 2 and 3 is zero, so finally

$$\mathbf{F}^3_{ji}=\mathbf{F}^3_8+\mathbf{F}^3_9. \tag{18}$$

Using this with (13) it is easy to check that

$$\mathbf{F}^3_{ij}=-\mathbf{F}^3_{ji}. \tag{19}$$

Calculation of the torque $\mathbf{M}^3_{ij}$ is possible after defining the direction of the interatomic 3–body forces. It can be noted, that atom of *Mo* with index 1 participates in all interactions (see Fig. 3). From (13) and (44) it follows, that any force $\mathbf{F}_{1\alpha\beta}$ can be represented as

$$\mathbf{F}_{1\alpha\beta}=\mu\mathbf{r}_{1\alpha}+\nu\mathbf{r}_{1\beta}, \tag{20}$$

where μ and ν are the coefficients that can be determined from (13). The similar relations can be obtained for $\mathbf{F}_{\alpha1\beta}$. Due to this, the directions of the forces are connected with the atom 1, hence the torque can be found as

$$\mathbf{M}^3_{ij}=\mathbf{r}_{i1}\times\mathbf{F}^3_1+\mathbf{r}_{i1}\times\mathbf{F}^3_4+\mathbf{r}_{i1}\times\mathbf{F}^3_5+\mathbf{r}_{i1}\times\mathbf{F}^3_6+\mathbf{r}_{i1}\times\mathbf{F}^3_7. \tag{21}$$

As it was mentioned above, some of these forces are equal to zero, so

$$\mathbf{M}^3_{ij}=\mathbf{r}_{i1}\times\mathbf{F}^3_1=\mathbf{r}_{i1}\times\mathbf{F}^3_{ij} \tag{22}$$

In turn, the three–body torque acting to the other grain with respect to its center is

$$\begin{aligned}\mathbf{M}^3_{ji} &= \mathbf{r}_{j1}\times\mathbf{F}^3_2+\mathbf{r}_{j1}\times\mathbf{F}^3_3+\mathbf{r}_{j1}\times\mathbf{F}^3_8+\mathbf{r}_{j1}\times\mathbf{F}^3_9\\ &= \mathbf{r}_{j1}\times\mathbf{F}^3_8+\mathbf{r}_{j1}\times\mathbf{F}^3_9.\end{aligned} \tag{23}$$

Taking (19) into account, it is possible to obtain the connection between the torques:

$$\mathbf{M}^3_{ij}+\mathbf{M}^3_{ji}=(\mathbf{r}_{i1}-\mathbf{r}_{j1})\times\mathbf{F}^3_{ij}=\mathbf{r}_{ij}\times\mathbf{F}^3_{ij}. \tag{24}$$

One can notice that in this case the third Newton's law for the torques is also satisfied.

3. Simulation technique

3.1. Dynamics of the grains

The forces and torques defined in the previous section are applied for the particle dynamics simulations. The main idea of the simulations method is close to the discrete [6] and distinct [12] element methods and other generalizations of classical molecular dynamics. As it was noted earlier, grains are simulated as the rigid bodies with the masses and moments of inertia determined by (1). The position of the center of mass of a specific grain i is determined by the solution of the following equation of motion:

$$m_i\ddot{\mathbf{u}}_i=\sum_{i\neq j}\left(\mathbf{F}^2_{ij}+\mathbf{F}^3_{ij}\right), \tag{25}$$

Rotation of the grain i is described as

$$\boldsymbol{\Theta}_i\cdot(\omega_i)^{\cdot}=\sum_{i\neq j}\left(\mathbf{M}^2_{ij}+\mathbf{M}^3_{ij}\right), \tag{26}$$

where $\omega_i=\omega_i\mathbf{w}_i$ is an angular velocity. A unit vector $\mathbf{w}_i$ determines the axis of rotation at current time step. The components of angular velocity vector can be found from integration of (26). Using it, we apply the quaternions formalism [2] to calculate a new orientation of the grain. Rotation around the vector $\mathbf{w}_i$ is calculated at each time step dt using quaternions $\mathbf{q}_i$:

$$\begin{aligned}\mathbf{q}_i(t+\mathrm{d}t) &= \mathbf{q}_i(t)*\mathrm{d}\mathbf{q}_i,\\ \mathrm{d}\mathbf{q}_i &= \cos\left(\frac{\omega_i\mathrm{d}t}{2}\right)+\mathbf{w}_i\sin\left(\frac{\omega_i\mathrm{d}t}{2}\right).\end{aligned} \tag{27}$$

For small rotations, this formula can be simplified:

$$\mathrm{d}\mathbf{q}_i=1-\frac{1}{2}\left(\frac{\omega_\mathbf{i}\mathrm{d}t}{2}\right)^2+\omega_\mathbf{i}\frac{\mathrm{d}t}{2}. \tag{28}$$

Additionally, quaternion $\mathbf{q}_i$ is normalized at every step.

We define vectors $\mathbf{r}_{i\alpha}$ as the position vectors connecting the i grain's center of mass with the *Mo* and *S* atoms inside this grain noted with α index. These vectors can be determined by the following relation

$$\mathbf{r}_{i\alpha}(t+\mathrm{d}t)=\mathbf{q}_i*\mathbf{r}_{i\alpha}(t)*\mathbf{q}_i^{-1}. \tag{29}$$

The Eqs. (25) and (26) are integrated at each step using leap–frog algorithm [1].

Table 1
Components of stiffness tensor of the lattice. C^1_{ij} for atomic $SLMoS_2$ with parameters of SW potential [9], C^2_{ij} for grain–structured $SLMoS_2$ with parameters of SW potential [9], C^3_{ij} for grain–structured $SLMoS_2$ with new parameters (Table 2).

	C^1_{ij}, GPa	C^2_{ij}, GPa	Relative error, %	C^3_{ij}, GPa	Relative error, %
C_{11}	284	644	124	284	0
C_{12}	82.3	168	104	73.2	11
C_{66}	101	238	135	105	4

3.2. Elasticity of the CG–lattice

In this section, we determine the parameters of interaction. As the grains are rigid, the overall stiffness of the lattice increased and we cannot use the original SW potential. Instead we need to redefine its parameters. In order to determine the components of stiffness tensor we need to solve a set of problems in which the material is subject to homogeneous strain field with one non-zero component. We write the Hooke's law in the form

$$\frac{\Delta\sigma_{kl}}{\Delta\varepsilon_{ij}} = \frac{1}{2}\left(C_{klij} + C_{ijkl}\right), \qquad i,j,k,l = x,y,z, \tag{30}$$

where ε_{ij} and σ_{kl} are the components of strain and Cauchy stress tensors respectively, and C_{ijkl} are the components of stiffness tensor. The problems are solved using central differences for $\varepsilon_{ij} = \pm 10^{-5}$, and consequently $\Delta\varepsilon_{ij} = 2\cdot 10^{-5}$. The boundary effects in the plane of isotropy are eliminated by introduction of periodic boundary conditions, whereas the upper and lower boundaries are free.

Further, Voigt notation is introduced for the stiffness tensor indices: *xx* is replaced by 1, *yy* and *zz* are replaced by 2 and 3 respectively, whereas *yz, xz* and *xy* become 4, 5 and 6.

The non-zero components of stiffness tensor are determined by the appearance of non-zero components of stress tensor as the result of the imposed strain. Note, that instead the original complex 3D lattice the coarse-grained lattice of grains is two–dimensional triangular one. A lattice of such kind is isotropic, so its tensor of stiffness has only 5 non-zero components: $C_{11} = C_{22}$, $C_{12} = C_{21}$, and C_{66}. These components were calculated for the original lattice using the SW proposed in [9](see Table 1). We use the Cauchy stress tensor calculated as

$$\sigma = \frac{1}{2V}\sum_{\alpha} \mathbf{a}_\alpha \mathbf{F}_\alpha, \tag{31}$$

where V is the actual unit cell volume, $\mathbf{F}_\alpha$ are the respective interatomic forces, and $\mathbf{a}_\alpha$ are the vectors connecting the given atom with its neighbors (see e.g. [3,7] and the references therein)

A Simulated Annealing (SA) algorithm [5] was used to determine the parameters of the SW potential using the known values of the stiffness tensor. The idea of the algorithm is the following. At each time step, the algorithm randomly selects parameters of SW potential ε, a and B close to the current ones. Then, a sum of absolute values of relative parameters deviations is calculated:

$$f(C_{ij}) = \sum_{ij} \frac{|C^1_{ij} - C^{current}_{ij}|}{C^1_{ij}}, \tag{32}$$

where C^1_{ij} are the components of stiffness tensor for original $SLMoS_2$ lattice with parameters of Stillinger-Weber potential [9]. Our goal is to find a minimum of this function. Based on the new value of the function, the algorithm decides whether to accept the new parameters or to stay with the current solution. The obtained elastic components and their relative deviation from the C^1_{ij} are shown in Table 1. Here C^2_{ij} are the values calculated for the coarse–grained lattice with the original SW parameters, and C^3_{ij} are those obtained with the parameters optimized using the SA algorithm.

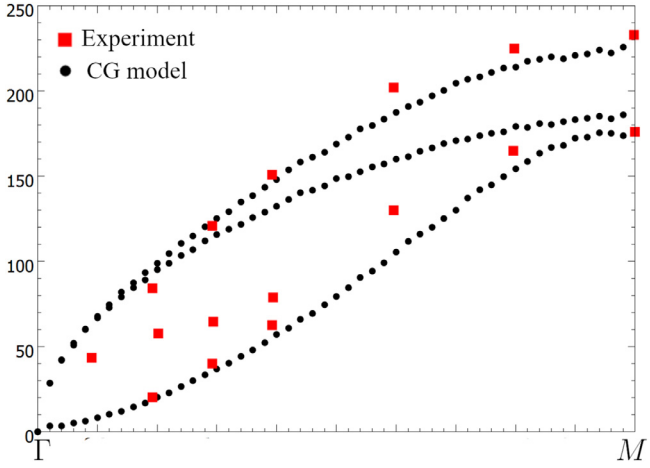

Fig. 4. Phonon spectrum for grain–structured $SLMoS_2$ with the new parameters (Table 2).

The corrected SW potential parameters for coarse–grained model are given in Table 2.

4. Applications

We have developed a CG–model of $SLMoS_2$ and the parameters of interaction between the grains have been determined. The next step is to check the possible applications of the model for two test problems: (i) determination of the phonon spectrum of the lattice, and (ii) nanoindentation experiment.

4.1. Phonon spectrum

The parameters of the model were determined using the quasistatic approach based on elastic properties calculations. A phonon spectrum determination can be used to validate the system dynamics. Phonon spectrum of the coarse–grained lattice is measured using an approach based on molecular dynamics simulations [10]. Note, that the general approach proposed in [10] can be simplified in our case. Indeed, the grains in $SLMoS_2$ crystal form a 2D triangular lattice. The primitive cell of such lattice is simple. As a result, the optical waves degrade, and the resulting phonon spectrum has only three acoustic waves.

The displacements in the reciprocal space are defined as the Fourier transform of displacements in the real space

$$\mathbf{u}(\mathbf{q}) = \frac{1}{\sqrt{N}}\sum_i \mathbf{u}_i \exp^{-i\mathbf{q}\cdot\mathbf{r}_i} \tag{33}$$

where N is a number of grains, $\mathbf{u}_i$ is a displacement of grain i, $\mathbf{q}$ is a wave vector.

The Green's tensor is calculated as a time average of the tensor product $\mathbf{u}(\mathbf{q})$ with a complex conjugate $\mathbf{u}^*(\mathbf{q})$

$$\mathbf{G}(\mathbf{q}) = \langle \mathbf{u}(\mathbf{q})\mathbf{u}^*(\mathbf{q})\rangle \tag{34}$$

Finally, the dynamical tensor $\mathbf{D}(\mathbf{q})$ is inverse to $\mathbf{G}(\mathbf{q})$ multiplied by the coefficient:

$$\mathbf{D}(\mathbf{q}) = \frac{1}{m}k_B T\left[\mathbf{G}^{-1}(\mathbf{q})\right] \tag{35}$$

where k_B is the Boltzmann constant, and T is the temperature.

Phonon dispersion curves are obtained by solving the eigenvalues problem for $\mathbf{D}(\mathbf{q})$ for different $\mathbf{q}$. The results are shown in a Fig. 4.

Even though we consider the phonon spectrum of grains instead of atoms, we obtain a good agreement with the experimental

Table 2
Re-calibrated Stillinger-Weber potential parameters.

	ε, eV	σ, Å	a	B	λ	γ	$\cos(\Theta_0)$
$Mo-Mo$	2.4436	0.6097	7.54817	119.751	0	0	0
$S-S$	4.1082	0.6501	6.06338	103.629	0	0	0
$Mo-S$	3.0014	0.7590	4.38728	37.8703	0	0	0
$Mo-S-S$	3.0014	0.7590	4.38728	37.8703	1.02384	0.872786	0.1525
$S-Mo-Mo$	3.0014	0.7590	4.38728	37.8703	1.02384	0.872786	0.1525

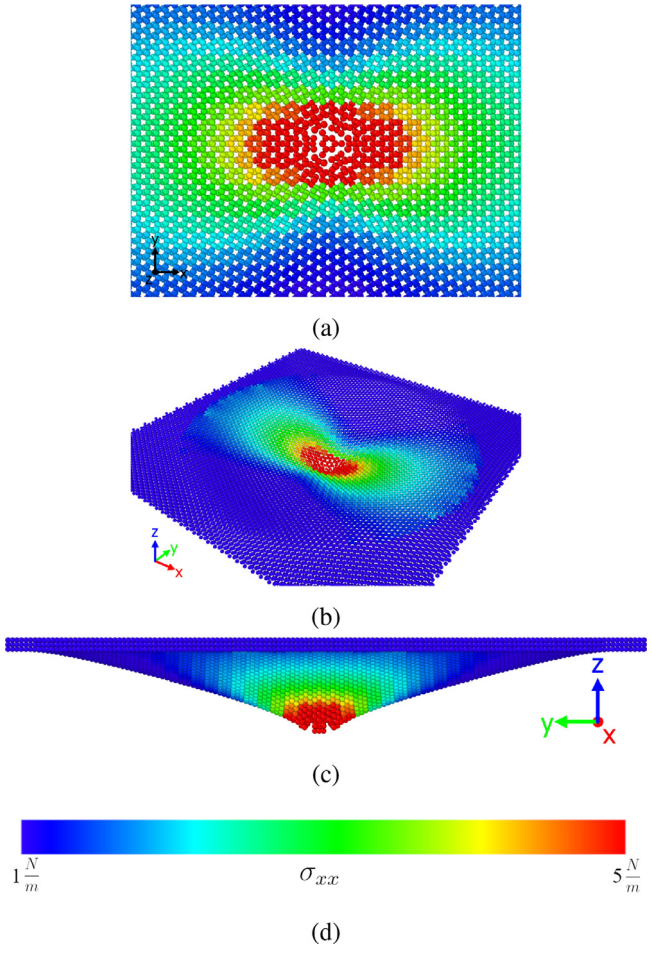

Fig. 5. Simulation of nanoindentation in $SLMoS_2$ using CG–model. Top view (a), isometric view (b), side view (c). The color corresponds to a σ_{xx} stress (d).

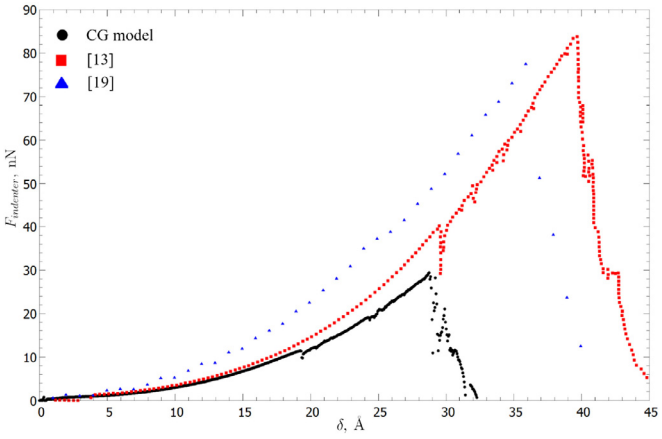

Fig. 6. Indentation procedure of $SLMoS_2$.

results. The lower and upper curves give a good approximation of experimental data from [17]. The middle curve varies significantly from the experimental data in case of long waves, but the difference decreases at higher values of the wave vector.

4.2. Nanoindentation

A circular region around central grain with radius of 100Å was chosen for indentation procedure on a square plate of $SLMoS_2$ (see Fig. 5). All grains beyond this radius were fixed both in terms of translational and rotational degrees of freedom. Grains, that were within 10Å radius from the indenter center, were assumed to interact with the indenter by a repulsive force like Lennard–Jones repulsive term. The spherical indenter was initially placed 10Å above the upper border of the plate and was moving with constant velocity of 0.1Å/*ps* along z-axis. Temperature of the system was sustained equal to 0.2*K*. These conditions are similar to those in calculations made by Wang [20] and Pang [13] for atomic $SLMoS_2$ with REBO potential. The only difference lies in the indenter velocity, that was equal to 0.2Å/*ps* in [13].

Fig. (6) shows the comparative results of the indentation carried out in this work (black circles), in [20] (blue triangles) and in [13] (red squares). At the first stage of indentation, the behavior predicted by our simulations is similar to that of [13]. After the deflection $\delta < 20$Å the deviation between the atomistic and coarse–grained models increases. The maximum possible deflection given by coarse–grained model is about 29Å which is lower than the one given by Wang model (~ 37Å) or Pang model (~ 41Å). This effect has the following explanation. Although the overall stiffness of the CG–lattice and atomic lattice are the same, on a microscopic level they are different. The grains in CG–lattice are rigid, so the bonds between them must have larger elongations than the corresponding bonds in atomic lattice. This leads to the higher stresses in the bonds and as a result, decreases the critical deflection of indentation. Thus, CG–model, proposed in this work, is valid primarily in linear stain regime.

5. Conclusions

We developed a coarse–grained model of $SLMoS_2$ with the grains considered as rigid bodies. For this specific study, the interactions between the grains were based on Stillinger–Weber potential with the parameters re-calibrated to fulfill the elastic properties of the original lattice. Note, that the same approach can be used with any other potential of interaction. The phonon spectrum was calculated, and it shows a good correspondence to the acoustic waves of the original lattice.

In this work, we considered the minimal possible grains. In this case, the number of interaction reduces almost twice. The larger grains with the same geometry can be used for the higher increase of the calculation speed.

The major advantage of the model is an opportunity to combine the coarse–grained and the original lattices in one model. For example, the original lattice can be considered near the stress concentration points in the tasks of nanoindentation or crack initia-

tion, and the CG–lattice can be merged with the original on the relatively far distance from such points. In this paper, defect–free structure has been considered. However, the defects can be introduced naturally by adding or removing some particles from the lattice. It must be noted that in a coarse–grained structure the minimal size of the defect is limited by the size of the grain. If the atomic–size defects are considered, the CG–lattice needs first to be merged with the original lattice with the defects added to it.

The drawback of the model yields from its main feature: the rigid grains 'freeze' part of the interactions. As a result, the bonds between the grains are highly elongated in comparison with the ones in the original lattice at the same strain, which lead to higher stresses in the CG–lattice. This effect limits the application of the model for problems with large deformations. However, in the small strain cases such as elastic wave propagation, thermal tasks, and others the model can be used successfully. A possible solution to the aforementioned disadvantage may be considered by using elastic grains instead of rigid ones, which is a topic of further investigation.

The work was partially supported by the President of the Russian Federation (grant No. MK-1820.2017.1).

Declaration of Competing Interest

The authors declare that they have no known competing financial interests or personal relationships that could have appeared to influence the work reported in this paper.

Appendix

Let us calculate the first derivatives of Stillinger–Weber potential with respect to interparticle distance. The pair (36) and three-body (37) interaction potentials have the form:

$$\Pi_{\alpha\beta}(\mathbf{r}_{\alpha\beta}) = \varepsilon A\left(B\sigma^{p} {r_{\alpha\beta}}^{-p} - \sigma^{q} r_{\alpha\beta}^{-q}\right) e^{\left[\frac{\sigma}{r_{\alpha\beta}-a\sigma}\right]}, \tag{36}$$

$$\Pi^{3}_{\alpha\beta\gamma}(\mathbf{r}_{\alpha\beta}, \mathbf{r}_{\alpha\gamma}) = \varepsilon\lambda e^{\left[\frac{\gamma\sigma}{r_{\alpha\beta}-a\sigma}+\frac{\gamma\sigma}{r_{\alpha\gamma}-a\sigma}\right]}\Delta\cos\Theta^{2}_{\alpha\beta\gamma}, \tag{37}$$

where $r_{\alpha\beta}$ and $r_{\alpha\gamma}$ are distances between particles α and β and α and γ, respectively, and $\mathbf{r}_{\alpha\beta}\cdot\mathbf{r}_{\alpha\gamma} = r_{\alpha\beta}r_{\alpha\gamma}\cos\Theta_{\alpha\beta\gamma}$, and $\Delta\cos\Theta_{\alpha\beta\gamma} = (\cos\Theta_{\alpha\beta\gamma} - \cos\Theta_0)$, whereas all the other variables are the potential parameters, which are calibrated for the particular material.

These functions can be simplified taking the parameters for $SLMoS_2$ into account, i.e. $A = 1.0,\ q = 0,\ p = 4$:

$$\Pi_{\alpha\beta} = \varepsilon\left(B\left(\frac{\sigma}{r_{\alpha\beta}}\right)^{4} - 1\right) e^{\left[\frac{\sigma}{r_{\alpha\beta}-a\sigma}\right]}, \tag{38}$$

$$\Pi^{3}_{\alpha\beta\gamma} = \varepsilon\lambda e^{\left[\frac{\gamma\sigma}{r_{\alpha\beta}-a\sigma}+\frac{\gamma\sigma}{r_{\alpha\gamma}-a\sigma}\right]}\Delta\cos\Theta^{2}_{\alpha\beta\gamma}. \tag{39}$$

First, let us write down several auxiliary derivatives:

$$\frac{\partial r_{\alpha\beta}}{\partial\mathbf{r}_{\alpha\beta}} = \frac{\mathbf{r}_{\alpha\beta}}{r_{\alpha\beta}}, \qquad \frac{\partial r^{2}_{\alpha\beta}}{\partial\mathbf{r}_{\alpha\beta}} = 2\mathbf{r}_{\alpha\beta},$$
$$\frac{\partial r^{-4}_{\alpha\beta}}{\partial\mathbf{r}_{\alpha\beta}} = -4\mathbf{r}_{\alpha\beta}{r_{\alpha\beta}}^{-6}. \tag{40}$$

Next, we obtain the following set of equalities:

$$\frac{\partial\frac{\gamma\sigma}{(r_{\alpha\beta}-a\sigma)}}{\partial\mathbf{r}_{\alpha\beta}} = -\frac{\gamma\sigma}{\left(r_{\alpha\beta}-a\sigma\right)^{2} r_{\alpha\beta}}\mathbf{r}_{\alpha\beta} \equiv p^{0}_{\alpha\beta}\mathbf{r}_{\alpha\beta}$$
$$\frac{\partial\frac{\gamma\sigma}{(r_{\alpha\gamma}-a\sigma)}}{\partial\mathbf{r}_{\alpha\gamma}} = -\frac{\gamma\sigma}{\left(r_{\alpha\gamma}-a\sigma\right)^{2} r_{\alpha\gamma}}\mathbf{r}_{\alpha\gamma} \equiv p^{0}_{\alpha\gamma}\mathbf{r}_{\alpha\gamma}$$

$$\frac{\partial\cos\Theta_{\alpha\beta\gamma}}{\partial\mathbf{r}_{\alpha\beta}} = -\frac{\cos\Theta_{\alpha\beta\gamma}}{{r_{\alpha\beta}}^{2}}\mathbf{r}_{\alpha\beta} + \frac{1}{r_{\alpha\beta}r_{\alpha\gamma}}\mathbf{r}_{\alpha\gamma} \equiv \mathbf{n}_{\alpha\beta}$$
$$\frac{\partial\cos\Theta_{\alpha\beta\gamma}}{\partial\mathbf{r}_{\alpha\gamma}} = -\frac{\cos\Theta_{\alpha\beta\gamma}}{{r_{\alpha\gamma}}^{2}}\mathbf{r}_{\alpha\gamma} + \frac{1}{r_{\alpha\gamma}r_{\alpha\beta}}\mathbf{r}_{\alpha\beta} \equiv \mathbf{n}_{\alpha\gamma} \tag{41}$$

As the result, the derivative of (36) has the form:

$$\frac{\partial\Pi_{\alpha\beta}}{\partial\mathbf{r}_{\alpha\beta}} = -\varepsilon\left[\frac{4B\sigma^{4}}{r^{6}_{\alpha\beta}} + \frac{\sigma}{r_{\alpha\beta}\left(r_{\alpha\beta}-a\sigma\right)^{2}}\left(\frac{B\sigma^{4}}{r^{4}_{\alpha\beta}} - 1\right)\right] \times e^{\frac{\sigma}{r_{\alpha\beta}-a\sigma}}\mathbf{r}_{\alpha\beta}. \tag{42}$$

Passing over to three-body potential, we can write down

$$\frac{\partial\Pi^{3}_{\alpha\beta\gamma}}{\partial\mathbf{r}_{\alpha\beta}} = \varepsilon\lambda e^{\left[\frac{\gamma\sigma}{r_{\alpha\beta}-a\sigma}+\frac{\gamma\sigma}{r_{\alpha\gamma}-a\sigma}\right]}\Delta\cos\Theta^{2}_{\alpha\beta\gamma}\frac{\partial\frac{\gamma\sigma}{r_{\alpha\beta}-a\sigma}}{\partial\mathbf{r}_{\alpha\beta}} + 2\varepsilon\lambda e^{\left[\frac{\gamma\sigma}{r_{\alpha\beta}-a\sigma}+\frac{\gamma\sigma}{r_{\alpha\gamma}-a\sigma}\right]}\Delta\cos\Theta_{\alpha\beta\gamma}\frac{\partial\cos\Theta_{\alpha\beta\gamma}}{\partial\mathbf{r}_{\alpha\beta}}$$
$$= p^{1}_{\alpha\beta\gamma}\frac{\partial\frac{\gamma\sigma}{r_{\alpha\beta}-a\sigma}}{\partial\mathbf{r}_{\alpha\beta}} + p^{2}_{\alpha\beta\gamma}\frac{\partial\cos\Theta_{\alpha\beta\gamma}}{\partial\mathbf{r}_{\alpha\beta}} \tag{43}$$

which finally yields to:

$$\frac{\partial\Pi^{3}_{\alpha\beta\gamma}}{\partial\mathbf{r}_{\alpha\beta}} = p^{1}_{\alpha\beta\gamma}p^{0}_{\alpha\beta}\mathbf{r}_{\alpha\beta} + p^{2}_{\alpha\beta\gamma}\mathbf{n}_{\alpha\beta} \tag{44}$$

$$\frac{\partial\Pi^{3}_{\alpha\beta\gamma}}{\partial\mathbf{r}_{\alpha\gamma}} = p^{1}_{\alpha\beta\gamma}p^{0}_{\alpha\gamma}\mathbf{r}_{\alpha\gamma} + p^{2}_{\alpha\beta\gamma}\mathbf{n}_{\alpha\gamma} \tag{45}$$

where

$$p^{1}_{\alpha\beta\gamma} = \varepsilon\lambda e^{\left[\frac{\gamma\sigma}{r_{\alpha\beta}-a\sigma}+\frac{\gamma\sigma}{r_{\alpha\gamma}-a\sigma}\right]}\Delta\cos\Theta^{2}_{\alpha\beta\gamma}$$
$$p^{2}_{\alpha\beta\gamma} = 2\varepsilon\lambda e^{\left[\frac{\gamma\sigma}{r_{\alpha\beta}-a\sigma}+\frac{\gamma\sigma}{r_{\alpha\gamma}-a\sigma}\right]}\Delta\cos\Theta_{\alpha\beta\gamma}$$
$$p^{0}_{\alpha\beta} = -\frac{\gamma\sigma}{\left(r_{\alpha\beta}-a\sigma\right)^{2}r_{\alpha\beta}}$$
$$p^{0}_{\alpha\gamma} = -\frac{\gamma\sigma}{\left(r_{\alpha\gamma}-a\sigma\right)^{2}r_{\alpha\gamma}} \tag{46}$$

References

[1] M.P. Allen, D.J. Tildesley, Computer Simulation of Liquids, Oxford university press, 1989.
[2] S. Altmann, Rotations, Quaternions, and Double Groups, Clarendon Press, Oxford, 1986.
[3] I. Berinskii, A.Y. Panchenko, E. Podolskaya, Application of the pair torque interaction potential to simulate the elastic behavior of $SLMos_2$, Modell. Simul. Mater. Sci. Eng. 24 (4) (2016) 45003.
[4] S. Bertolazzi, D. Krasnozhon, A. Kis, Nonvolatile memory cells based on MoS_2/graphene heterostructures, ACS Nano 7 (4) (2013) 3246–3252, doi:10.1021/nn3059136.
[5] V. Černỳ, Thermodynamical approach to the traveling salesman problem: an efficient simulation algorithm, J. Optim. Theory Appl. 45 (1) (1985) 41–51.
[6] P.A. Cundall, O.D. Strack, A discrete numerical model for granular assemblies, Geotechnique 29 (1) (1979) 47–65.
[7] E. Ivanova, A. Krivtsov, N. Morozov, Derivation of macroscopic relations of the elasticity of complex crystal lattices taking into account the moment interactions at the microlevel, J. Appl. Math. Mech. 71 (4) (2007) 543–561, doi:10.1016/j.jappmathmech.2007.09.009.
[8] J.-W. Jiang, Graphene versus MoS_2: a short review, Front. Phys. 10 (3) (2015) 287–302, doi:10.1007/s11467-015-0459-z.
[9] J.-W. Jiang, H.S. Park, T. Rabczuk, Molecular dynamics simulations of single-layer molybdenum disulphide (MoS_2): Stillinger–Weber parametrization, mechanical properties, and thermal conductivity, J. Appl. Phys. 114 (6) (2013) 64307.
[10] L.T. Kong, Phonon dispersion measured directly from molecular dynamics simulations, Comput. Phys. Commun. 182 (10) (2011) 2201–2207.
[11] T. Lorenz, J.-O. Joswig, G. Seifert, Stretching and breaking of monolayer MoS_2an atomistic simulation, 2D Mater. 1 (1) (2014) 11007.
[12] I. Ostanin, R. Ballarini, D. Potyondy, T. Dumitrică, A distinct element method for large scale simulations of carbon nanotube assemblies, J. Mech. Phys. Solids 61 (3) (2013) 762–782.

[13] H. Pang, M. Li, C. Gao, H. Huang, W. Zhuo, J. Hu, Y. Wan, J. Luo, W. Wang, Phase transition of single-layer molybdenum disulfide nanosheets under mechanical loading based on molecular dynamics simulations, Materials 11 (4) (2018) 502.
[14] B. Radisavljevic, A. Radenovic, J. Brivio, V. Giacometti, A. Kis, Single-layer MoS_2 transistors, Nat. Nanotechnol. 6 (3) (2011) 147–150, doi:10.1038/nnano.2010.279.
[15] J.A. Stewart, D. Spearot, Atomistic simulations of nanoindentation on the basal plane of crystalline molybdenum disulfide (MoS_2), Model. Simul. Mater. Sci. Eng. 21 (4) (2013) 45003.
[16] A. Stukowski, Visualization and analysis of atomistic simulation data with OVITO-the Open Visualization Tool, Model. Simul. Mater. Sci. Eng. 18 (1) (2010), doi:10.1088/0965-0393/18/1/015012.
[17] N. Wakabayashi, H. Smith, R. Nicklow, Lattice dynamics of hexagonal MoS_2 studied by neutron scattering, Phys. Rev. B 12 (2) (1975) 659–663, doi:10.1103/PhysRevB.12.659.
[18] C.-X. Wang, C. Zhang, J.-W. Jiang, T. Rabczuk, A coarse-grained simulation for the folding of molybdenum disulphide, J. Phys. D Appl. Phys. 49 (2) (2015) 25302.
[19] C.-X. Wang, C. Zhang, T. Rabczuk, A two-dimensional coarse-grained model for molybdenum disulphide, J. Model. Mech. Mater. 1 (2) (2016).
[20] W. Wang, L. Li, C. Yang, R.A. Soler-Crespo, Z. Meng, M. Li, X. Zhang, S. Keten, H.D. Espinosa, Plasticity resulted from phase transformation for monolayer molybdenum disulfide film during nanoindentation simulations, Nanotechnology 28 (16) (2017) 164005.